FULL PAPER

Magnetic Resonance in Medicine 000:000–000 (2011)

Real-Time Optical Motion Correction for Diffusion Tensor Imaging

Murat Aksoy,[1] Christoph Forman,[1,2] Matus Straka,[1] Stefan Skare,[1,3] Samantha Holdsworth,[1] Joachim Hornegger,[2] and Roland Bammer[1]*

Head motion is a fundamental problem in brain MRI. The problem is further compounded in diffusion tensor imaging because of long acquisition times, and the sensitivity of the tensor computation to even small misregistration. To combat motion artifacts in diffusion tensor imaging, a novel real-time prospective motion correction method was introduced using an in-bore monovision system. The system consists of a camera mounted on the head coil and a self-encoded checkerboard marker that is attached to the patient's forehead. Our experiments showed that optical prospective motion correction is more effective at removing motion artifacts compared to image-based retrospective motion correction. Statistical analysis revealed a significant improvement in similarity between diffusion data acquired at different time points when prospective correction was used compared to retrospective correction ($P < 0.001$). Magn Reson Med 000:000–000, 2011. © 2010 Wiley-Liss, Inc.

Key words: motion; DTI; diffusion; real-time motion correction; optical motion correction; prospective motion correction

Diffusion tensor imaging has notoriously long acquisition times and, thus, successfully correcting for rigid head motion artifacts is key for both clinical exams and neuroscience studies, which is often overlooked. Particularly, with the more complex variants of diffusion tensor imaging (DTI), scan times increase excessively, which in turn leads to a higher likelihood of involuntary patient motion, even in subjects who comply and try to remain still. Additional complications arise when imaging children or patients with severe medical conditions (e.g., stroke or Parkinson's disease) that prevent them from staying stationary for even short times.

Gross patient motion during MRI exams results in spatial misregistration, which may cause blurring or complete loss of anatomical structures. With DTI, pixel misregistration also affects the shape of the diffusion tensor or orientation distribution functions. To mitigate misregistration artifacts, image-based retrospective methods have been suggested (1). These remedies are rather straightforward to apply for single-shot sequences and mostly involve retrospective volume-to-volume registration. However, retrospective volume-to-volume registration does not account for the influences of through-plane motion on local spin history. In addition, a whole motion-free volume must be acquired to perform reliable volume-to-volume registration because motion within the acquisition of a single volume (i.e., intravolume motion) will render the volume inconsistent. This can be particularly problematic for DTI where repetition times may approach 10 sec.

Apart from retrospective volume-to-volume registration methods, retrospective slice-to-volume registration is also used for motion correction in DTI (2). The performance of slice-to-volume registration is not degraded by intravolume motion. Nevertheless, this method is also susceptible to spin history effects. Slice-to-volume registration also restricts the minimum image resolution in the slice-select direction to guarantee sufficient sampling of the volume after motion correction.

With image-based retrospective methods, an adjustment of the **b** matrix for each rotated image is applied to correct for the directional encoding error (1). While changes in the **b** matrix can be corrected retrospectively, the distribution of diffusion-encoding directions that are effectively applied is suboptimal and can cause errors in the estimation of diffusion tensors or orientation distribution functions (3). Matters become ever more challenging for multishot sequences, such as PROPELLER (4) or SNAILS (5), where each profile/interleave can experience different motion. In fact, there is a great chance that each interleave is encoded with a different **b** matrix than originally prescribed. Therefore, it becomes impossible to reconstruct a diffusion-weighted image, which has a single defined diffusion-weighting direction (6).

In contrast, prospective correction techniques directly adapt scan geometry in (quasi) real-time to compensate for patient motion during data acquisition (7–10). A prospective approach would greatly overcome the aforementioned limitations of retrospective methods. One such method, prospective acquisition correction (9), registers each newly acquired volume to a template volume in real-time from which it determines pose changes, and feeds back the updated pose information to the sequencer

[1]Department of Radiology, Stanford University, Stanford, California, USA.

[2]Pattern Recognition Lab, Department of Computer Science, Friedrich-Alexander-University Erlangen-Nuremberg, Erlangen, Germany.

[3]Department of Clinical Neuroscience, Karolinska Institute, Stockholm, Sweden.

This work was presented in part at the 17th Scientific Meeting of the ISMRM, Honolulu, Hawaii, USA, 2009; ISMRM Workshop on Current Concepts of Motion Correction for MRI & MRS, Kitzbühel, Tyrol, Austria, 2010.

Grant sponsor: NIH; Grant numbers: 1R01EB008706, 5R01EB002711, 1R01EB006526, and 1R21EB006860; Grant sponsors: Center of Advanced MR Technology at Stanford; Grant number: P41RR09784; Grant sponsors: Lucas Foundation, Oak Foundation, GE Healthcare.

*Correspondence to: Roland Bammer, Ph.D., Department of Radiology, Lucas Center, Stanford University, 1201 Welch Road, Stanford, California 94305-5488. E-mail: rbammer@stanford.edu

Received 19 April 2010; revised 24 November 2010; accepted 2 December 2010.

DOI 10.1002/mrm.22787
Published online in Wiley Online Library (wileyonlinelibrary.com).

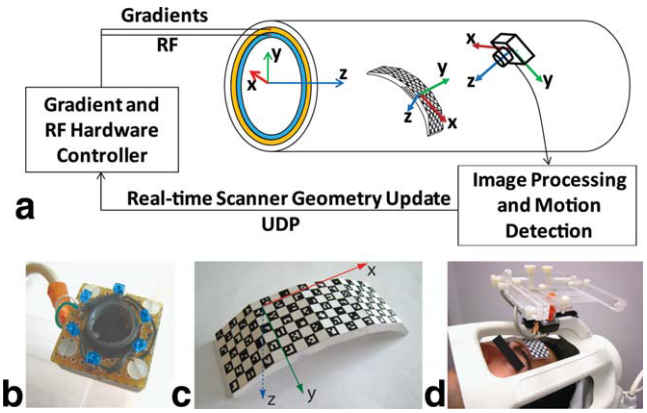

FIG. 1. System setup. An MR-compatible camera was mounted on the head coil inside the scanner bore (**b**). The camera took images of a self-encoded marker that was attached to the patient's forehead (**c**, **d**). These images were processed by an external laptop where (1) the marker was segmented out, (2) its pose was estimated, and (3) the six parameters (i.e., three rotations and three translations) to update the scanner geometry were sent to the scanner RF and gradient hardware controller. This allowed the slice being scanned to follow the subject's head in real-time. [Color figure can be viewed in the online issue, which is available at wileyonlinelibrary.com.]

so that the scanned plane follows patient motion. Although prospective acquisition correction addresses some of the challenges with retrospective volume-to-volume registration, it is still susceptible to intravolume motion and has a latency of one pulse repetition time (TR). Ultimately, all image-based registration methods have in general a degraded performance if the image signal level is low, which might happen for high b value scans.

Computer vision-based pose tracking is an effective variant to measure head movement that is compatible with prospective motion correction (10–12). This approach is particularly promising as it does not require any additional MR data acquisition (i.e., navigators) and is entirely independent from the regular MR imaging procedure. It also eliminates certain disadvantages related to retrospective or prospective image-based methods. Even for single-shot methods, it has been shown previously that prospective motion correction based on optical tracking (7) or active markers (8,13) perform superiorly to image-based retrospective or prospective correction, predominantly due to the considerably reduced spin history effects. Do note that, compared to conventional structural imaging, motion correction for diffusion-weighted MRI is considerably more challenging. For exact tensor estimation, motion-induced phase errors (14) and signal drop-outs (caused by motion in the presence of the strong diffusion-encoding gradient field) must also be considered.

In this study, our aims were: (1) to show the application of a prospective monovision-based optical tracking system (15) to perform rigid head motion correction and (2) to compare the effectiveness of retrospective and prospective motion correction for DTI.

THEORY AND METHODS

Prospective Motion Correction System Setup

The optical motion correction system is shown in Fig. 1. A single MR compatible camera (Fig. 1b) was mounted on an eight-channel phased array head coil (InVivo Corp., Gainesville, FL) (15). The camera acquired images of a self-encoded checkerboard marker with MR-visible features (Figs. 1c,d and 2) that was fixed to the patient's head. The images taken by the camera were then sent to an external processing laptop (IBM Lenovo, Inter Core 2 Duo CPU @ 2.80 GHz, 4GM RAM, 32-bit Windows Vista operating system), which was connected to the Gigabit Ethernet backbone of the MRI scanner. For every camera frame, each square on the checkerboard was segmented out and identified by a unique ID imprinted on it (16).

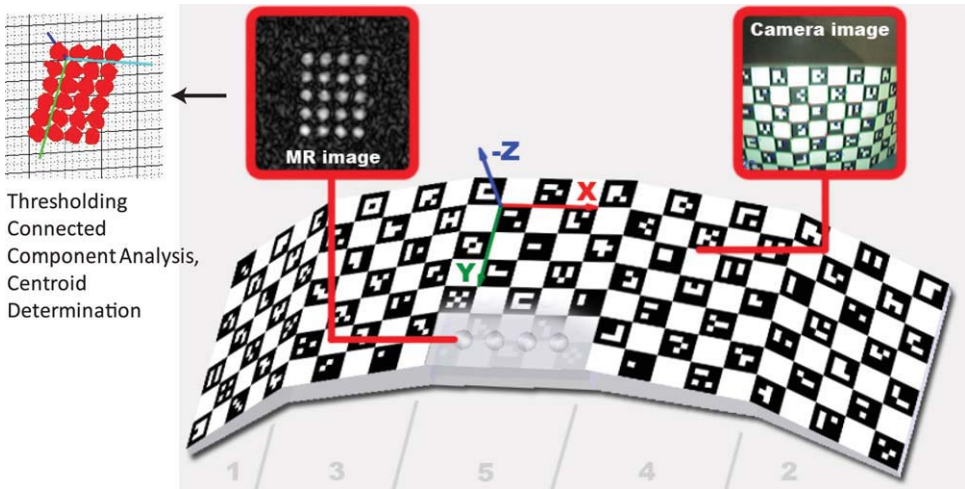

FIG. 2. The 3D self-encoded marker used for pose tracking. Each black square on the marker included a unique 2D barcode that represented the position of that square on the marker geometry. To perform cross-calibration, we also put MR-detectable agar droplets at the back of the marker. By measuring the poses of the MR-detectable agar filled holes and the self-encoded checkerboard pattern simultaneously by the scanner and the camera, it was possible to find the relation between the scanner and the camera frame of references. [Color figure can be viewed in the online issue, which is available at wileyonlinelibrary.com.]

This step was followed by the determination of the intersection points of the checkerboard squares. The detected grid point coordinates were then used as input to the 3D pose estimation algorithm (17). Here, the estimated pose of the marker allows one to get a geometry (i.e., slice position, orientation) update to be fed back to the scanner gradient and radio frequency (RF) hardware controller in real time. At the beginning of each patient study, a scanner–camera cross-calibration was performed to relate the camera–frame-of-reference to the scanner–frame-of-reference. A more detailed description of these steps is provided below.

Camera

Figure 1 shows the camera and rig used to mount the camera onto the coil. An off-the-shelf, small CMOS (380 TV lines, 1/3″ sensor) spy camera (Swann Communications USA Inc., CA) was optimized for MR-compatibility. Customized infrared light-emitting diodes were added on the front panel of the camera to illuminate the checkerboard inside the scanner and operated at an intensity level safe to the human eye.

Self-encoded Marker

To determine pose changes of the patient's head, the camera needs to track some feature points that are rigidly connected to the head. Due to the proximity between the marker and camera (5–7 cm), part of the marker can go outside of the camera's field-of-view (FOV) if large head motion occurs. If part of the marker is not visible to the camera, the positioning of the feature points with respect to each other cannot be determined. Occlusions of the marker can also occur due to the small gaps between rungs of the birdcage head coil.

A self-encoded marker was used to address these issues, as shown in Fig. 2. This marker was conceived and developed in-house and was built in the machine shop of our institution. A detailed description of this marker can be found in Ref. 16. The basis of this marker is a checkerboard pattern. Our custom modification consists of a rotationally invariant 2D-barcode inside each square of the checkerboard. Each barcode identifies the relative position of a given square within the checkerboard. This allows for accurate and robust pose tracking even with a partial view of the marker, thus allowing even larger head rotations than FOV supported by the camera to be detected. Moreover, the nonplanar marker geometry increased the pose detection accuracy over planar markers (specifically when marker plane is parallel to and directly facing the camera image plane, which is otherwise a challenge for other 2D markers; Ref. 18). Previous studies performed to measure the reproducibility (i.e., precision) of motion tracking have shown that, using this marker, the noise on the motion tracking data is on the order of 0.05 mm and 0.1° (16).

Scanner–Camera Cross-calibration

A cross-calibration procedure is necessary to determine the coordinate transform between camera-space where the checkerboard is tracked, and scanner-space, where the scan plane is prescribed. A fast calibration technique was developed, where a small-FOV 3D-SPGR (TR/echo time = 8.4/2.9 msec, 128 × 128 × 48 resolution, FOV = 12 cm, slice thickness = 1 mm, NEX = 2, scan time = 52 sec) was used to map the agar-filled holes embedded underneath the checkerboard, while the camera simultaneously observed the checkerboard surface (Fig. 2). The information collected from the scanner and the camera was then used to calculate the cross-calibration transformation matrices, which is described in the next section. The pose estimation error (i.e., the accuracy) of the combination of motion tracking and cross-calibration was below 1 mm and 1° in a range of ∼20° motion (16).

Mathematical Description

The mathematical description of optical prospective motion correction was presented previously (10) and is briefly reviewed here. Let c denote the camera frame of reference, m_0 the initial marker position, m_i the marker position at time i, s_0 the initial scan plane position, s_i the scan plane position at time i. Let $\mathbf{T}$ be a 4 × 4 transformation matrix that consists of a 3 × 3 rotation matrix $\mathbf{R}$ and 3 × 1 translation vector $\mathbf{t}$

$$\mathbf{T} = \begin{bmatrix} \mathbf{R} & \mathbf{t} \\ 0\ \ 0\ \ 0 & 1 \end{bmatrix} \tag{1}$$

The purpose of prospective motion correction is to make sure that the rotation and translation between the scanned volume and the marker stays constant for each point (i) in time. This is described mathematically as:

$$\mathbf{T}_{m_0 \to s_0} = \mathbf{T}_{m_i \to s_i} \tag{2}$$

With straightforward matrix manipulations, the following can be obtained:

$$\begin{aligned} \mathbf{T}_{m_0 \to s_0} &= \mathbf{T}_{m_i \to s_i} \\ \mathbf{T}_{c \to s_0} \mathbf{T}_{m_0 \to c} &= \mathbf{T}_{s_0 \to s_i} \mathbf{T}_{c \to s_0} \mathbf{T}_{m_i \to c} \\ \mathbf{T}_{s_0 \to s_i} &= \mathbf{T}_{c \to s_0} \mathbf{T}_{m_0 \to c} \mathbf{T}_{c \to m_i} \mathbf{T}_{s_0 \to c} \end{aligned} \tag{3}$$

$\mathbf{T}_{s_0 \to s_i}$ represents the geometry update that needs to be applied to the scanned volume in real time for motion correction. $\mathbf{T}_{c \to s_0}$ is the scanner–camera cross-calibration matrix and is obtained using the method described in the previous section. $\mathbf{T}_{m_0 \to c}$ and $\mathbf{T}_{m_i \to c}$ are the marker positions with respect to the camera at time 0 and time i. These marker positions are obtained using the principles of computer vision and a perspective camera model as described above and in Refs. 16,17.

Experiments

All in vivo experiments were carried out using a 1.5 T GE Signa scanner (GE Healthcare, Software Release 15.0

M4, with a maximum gradient strength of 40 mT/m and a slew rate of 150 T/m/sec). All human subjects' experiments were approved by the institutional review board at our university (Protocol ID: 10774). With written informed consent, three male volunteers (age 27–30) were scanned for this study. Before each session, all subjects practiced for the motion experiments to guarantee reproducibility of motion patterns.

In Vivo DTI Experiments, 96 × 96 Resolution, Single-Shot EPI Readout

A single-shot DTI sequence with echo-planar imaging (EPI) readout with the following parameters was used: TR/echo time = 10,000 msec/75 msec, FOV = 24 cm, 96 × 96 acquisition resolution, half-Fourier readout with 20 overscans, 36 slices, slice thickness = 3 mm, 1 mm gap, b = 1000 sec/mm^2, number of diffusion-encoding directions = 25 (+3 b = 0 acquisitions), total scan time = 4:40 min. For this experiment, the volunteer was asked to perform mixed shaking (predominantly in-plane) and nodding (predominantly through-plane) motion throughout the scan once every ~ 15 sec. This was repeated with the prospective motion correction system turned off and on. The shaking and nodding data sets with no active prospective motion correction were also reconstructed after volume-to-volume realignment using Statistical Parametric Mapping (SPM, version 5.0) software. To get reference data and to observe the effects of prospective motion correction on motion-free data, two additional scans were performed where the volunteer was asked to lie still while prospective motion correction system was again either turned off or on. Thus, a total of five data sets were obtained: (1) (reference data set) no motion—no correction; (2) no motion—prospective correction; (3) shaking and nodding motion—no correction; (4) shaking and nodding motion—retrospective correction (i.e., volume-to-volume realignment); (5) shaking and nodding motion—prospective correction. The slices with low average signal levels were removed from DTI analysis prior to reconstruction of tensors. For each data set, fiber tractography was performed using a custom-built software (19). Seed regions were placed and saved for the corpus callosum and both cortico-spinal tracts so that they could be applied reliably for each of the five data sets. Euler's method was used for tracking with fractional anisotropy (FA) threshold = 0.15 and curvature threshold = 40°.

In Vivo DTI Experiments, 128 × 128 Resolution, Multishot Spiral Readout

Here, a constant-density multishot spiral-in and variable-density spiral-out pulse sequence was used (6). Specifically, the variable-density spiral-out part contributed one spiral arm of the final high-resolution diffusion-weighted image, while corresponding to each spiral-out arm the constant-density spiral-in part provided a low-resolution navigator image that was sampled at Nyquist rate. These spiral-in navigators were used for two purposes: (1) correction of the nonlinear phase variation caused by motion during diffusion encoding (14), as described by Liu et al. (20), and (2) estimation of (in-plane) 2D pose changes between spiral-out interleaves for retrospective 2D motion correction. To estimate the pose changes between interleaved acquisitions, individual low-resolution navigators were (rigidly) coregistered to a template by minimizing the Pearson cross-correlation coefficient between the template navigator image and the navigator image to be registered. The robustness of this approach has been demonstrated in a recent study (21). The following acquisition parameters were used: TR/echo time = 3000 msec/55 msec, FOV = 24 cm, 128 × 128 acquisition resolution, variable-density spiral-out readout with a pitch factor α = 3.0 (22), eight spiral interleaves, 13 slices, slice thickness=5 mm, 1 mm gap, b = 800 sec/mm^2, number of diffusion-encoding directions = 6 (+1 b = 0 acquisition), NEX = 2, spiral-in navigator acquisition resolution: 32 × 32. Total scan time was 5:36 min. The acquisition matrix was comparable to regular single-shot scanning but with a roughly 8-fold reduction in image distortion due to the interleaved spiral acquisition.

Similar to the previous case, seven data sets were obtained with this study: (1) (reference data set) no motion—no correction; (2) shaking motion—no correction; (3) shaking motion—retrospective 2D correction (as described above); (4) shaking motion—prospective correction; (5) nodding motion—no correction; (6) nodding motion—retrospective 2D correction; (7) nodding motion—prospective correction.

All reconstructions were performed using augmented SENSE reconstruction and nonlinear phase correction (20). To compare the performance of retrospective and prospective methods, the following analyses were performed. Each method was applied separately to data sets 2–7 separately.

Angular deviation maps. As a metric for consistency of directional diffusion encoding, the pixelwise angular deviation of the reconstructed primary eigenvectors relative to the eigenvectors of the reference data set (i.e., no motion, no correction) was obtained for each reconstructed data set (6). The angular deviation was measured by taking the scalar product between the test and reference eigenvector for each voxel. On these deviation maps, region-of-interest (ROI) analyses were performed for the splenium of corpus callosum. As uncorrected motion will also affect the accuracy of the directional information in the tensor, a lower angular deviation will be an indicator of a more successful motion correction. To facilitate better interpretation of these maps, we also obtained two reference angular deviation maps between (1) no motion and no correction—no motion and no correction; and (2) no motion and no correction—no motion and prospective correction scans.

Distribution of correlation coefficients between navigators. The low-resolution spiral-in navigator images were obtained for each interleave (112 images = 8 interleaves × 14 directions) and a template image was formed by coregistering and averaging all navigators. Thereafter, the Pearson correlation coefficient between each individual navigator and this template was calculated for each of the three groups (no correction, retrospective correction, and prospective correction). A Mann–Whitney U test was performed to investigate whether the correlation coefficients between the retrospectively corrected and

prospectively corrected groups differed significantly using the hypothesis that prospective motion correction allowed for greater data consistency (as indicated by a higher correlation coefficient). To visualize the distribution of the correlation coefficients of the navigators, box and whisker plots were used. Specifically, for each box plot, the center of the box represented the median and the edges were the 25 and 75 percentiles. The whiskers indicated range of correlation values that were not considered to be outliers. This test was repeated for the shaking and nodding motion experiment.

Variance maps. To eliminate the effect caused by contrast differences between navigator images that were acquired with diffusion weighting applied along different encoding directions, only navigator images obtained with $b = 0$ were analyzed. Specifically, from 16 $b = 0$ navigator images (eight interleaves, NEX = 2) the signal variance was computed across all 16 time points for each pixel.

In Vivo DWI Experiments, 256 × 256 High-Resolution, Multishot Spiral Readout

A high-resolution spiral diffusion-weighted imaging (DWI) scan was performed using the following parameters: TR/echo time =4000 msec/55 msec, FOV=24 cm, 256 × 256 acquisition resolution, variable-density spiral-out readout with a pitch factor $\alpha = 3.0$, 24 spiral interleaves, 13 slices, slice thickness= 5 mm, 1 mm gap, $b = 800$ sec/mm^2, diffusion-encoding directions = 3, NEX = 1, spiral-in navigator acquisition resolution: 32 × 32. Without loss of generality and in the interest how much time the subjects spent in total in the magnet, only diffusion-weighted scans were performed along the three principal axes. Reconstruction and retrospective 2D correction were done using the methods described for the 128 × 128 experiment. The volunteer was asked to perform mixed shaking and nodding motion throughout the scan. A total of five data sets were obtained: (1) (reference data set) no motion—no correction; (2) no motion—prospective correction; (3) shaking and nodding motion—no correction; (4) shaking and nodding motion—restrospective 2D correction; (5) shaking and nodding motion—prospective correction.

As a quality metric to measure the amount of motion artifacts, we used the signal energy in the high frequency power spectrum of *k*-space (8). This was calculated by taking the sum-of-squares of *k*-space points above a cut-off frequency (cut-off = 2.6 rad/cm). For objects containing sharp edges and small structures (i.e., human brain), motion is expected to cause blurring and loss of edge structures in image space, which is reflected in a decrease in energy at high spatial frequencies in *k*-space (since high spatial frequencies mostly contain edge information). Thus, higher energy at high spatial frequencies is an indication of less motion artifacts. To eliminate the energy differences between different scans that may arise due to different prescan values, the images were first normalized by the mean image intensity of the middle slice for all five data sets. The high frequency energy of each slice was then represented as a percentage relative to the reference volume.

RESULTS

In Vivo DTI Experiments, 96 × 96 Resolution, Single-Shot EPI Readout

Figure 3a shows the axial, sagittal, and coronal FA maps, and Fig. 3b shows the fiber tracts obtained for five different data sets. The range of motion detected by the optical system was 6° and 6 mm, and the occurrence of motion was once per ~ 15 sec. The noncorrected FA maps show detrimental motion artifacts. Retrospective correction using volume-to-volume realignment improved the image quality, but artifacts still remained mainly due to intravolume motion and spin history effects. The data set with prospective motion correction showed the highest degree of similarity with the data with no motion. The reconstructed fiber pathways also reveal that prospective motion correction provided better visualization of cortico-spinal tracts compared to retrospective correction (Fig. 3b, yellow arrow). For the two scans where the subject was instructed to stay still, visualization of cortico-spinal tracts was also better for prospectively corrected data compared to noncorrected data. This was due to the fact that, despite the subject was to remain still for the nonmotion data set, a small amount of motion was still detected (~ 1.5° and ~ 1 mm drift throughout the scan). Thus, running prospective motion correction on the noncorrupted data set still improved the data quality.

In Vivo DTI Experiments, 128 × 128 Resolution, Multishot

FA and Mean Diffusion Images

Figure 4a–c shows the in vivo experiments in which the subjects were asked to perform either shaking or nodding motion during the course of the DTI exam. Figure 5 shows the volunteer motion as measured by the optical system. As anticipated, without any motion correction, there were significant motion artifacts on both iso-DWI images and the FA maps that severely degraded image interpretation (Fig. 4a,b).

For the experiment with left-right head rotation, retrospective correction cleared out some of the artifacts. However, for head rotation the volunteers also typically performed some involuntary through-plane motion (see Fig. 5). As our retrospective 2D-correction algorithm only corrects for in-plane motion, residual artifacts remained due to unaccounted through-plane motion components. Conversely, the images reconstructed with prospective motion correction appeared visually of higher quality compared to images reconstructed with retrospective correction.

For the DTI experiment with the subject nodding, no significant improvement in image quality was observed after the application of retrospective in-plane motion correction (Fig. 4a,b). Again, this is due to the inability of 2D retrospective motion correction to correct through-plane motion and demonstrates the limitations of 2D acquisition methods that rely solely on in-plane motion correction (4–6,23). The application of prospective motion correction provided a significant improvement in image quality.

Angular Deviation Maps

Figure 4c and Table 1 show the deviation of the major eigenvectors from their true orientations inside an ROI

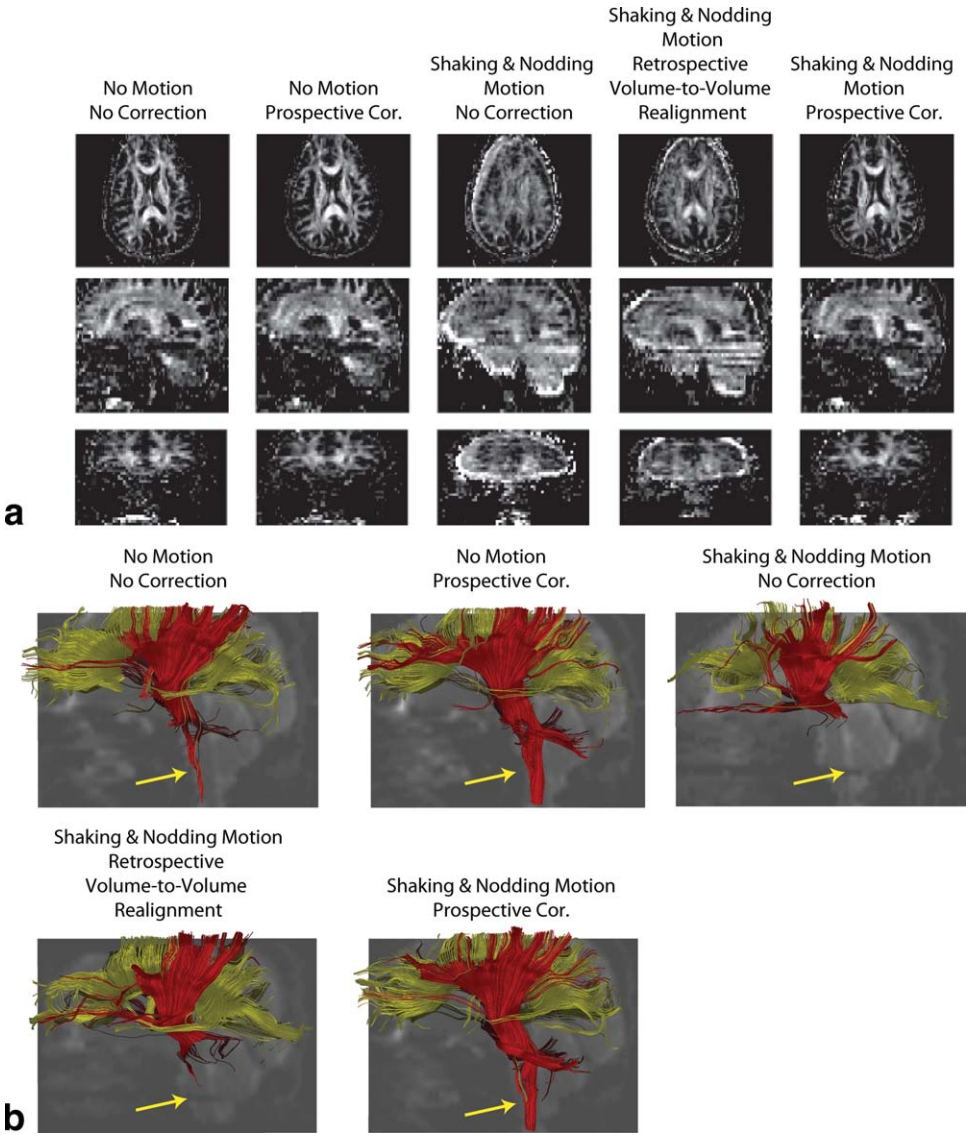

FIG. 3. Results of in vivo DTI experiments with 96 × 96 single-shot EPI readout. Reconstructed FA maps show that, even with retrospective volume-to-volume realignment, motion-related image artifacts remain because of intravolume motion and spin history effects. Prospectively corrected FA maps show the most similarity with the reference data set. The visualization of corticospinal tracts was also more successful when prospective correction was used compared to retrospectively corrected data set.

containing the splenium of the corpus callosum. The true orientations were given by the nonmotion corrupted data set. The error in the orientation of the major eigenvectors is the largest when motion was not corrected (Fig. 4c). The angular error inside the ROI was 10.14 ± 6.32° for in-plane motion and 6.02 ± 3.83° for nodding motion. For the experiment including in-plane rotation, prospective correction performed similar (7.38 ± 4.99 vs. 7.02 ± 4.81° mean deviation). The difference between prospective and retrospective correction was more pronounced in the presence of nodding motion (5.3 ± 2.99 vs. 3.29 ± 1.63° deviation). The residual angular deviation after motion correction was significantly larger for the in-plane versus through-plane case as the possible range of shaking motion (±15°) was more than the range of nodding motion (±10°; Fig. 4d) because of the restricted area in the head coil. Thus, the secondary effects of motion (e.g., susceptibility effects, gradient nonlinearities, etc.) were more pronounced in the shaking motion images. In addition, independent of the range of motion possible, the change in effective coil sensitivity was also greater for shaking versus nodding motion due to the coil geometry (that is, the coil sensitivity variation is more pronounced in the R/L direction compared to S/I direction).

To provide reference values for Table 1, scans with the volunteer lying still were acquired. The mean angular deviation between two "no motion" scans with "no correction" was 2.55 ± 1.47°. The mean angular deviation between the "no motion, no correction" and "no motion, prospective correction" scan was 2.39 ± 1.43°. Note that the high standard deviation of the angular deviations shown in Table 1 is due to the inherent sensitivity of the reconstructed eigenvectors to small signal fluctuations which might be caused by off-resonance effects or coil sensitivity changes. Thus, the values in Table 1 should be evaluated in connection with the angular deviation maps given in Fig. 4c.

Distribution of Correlation Coefficients Between Navigators

The Mann–Whitney U test revealed statistically significant differences between retrospectively and prospectively corrected groups ($P < 0.001$). Figure 6a shows the

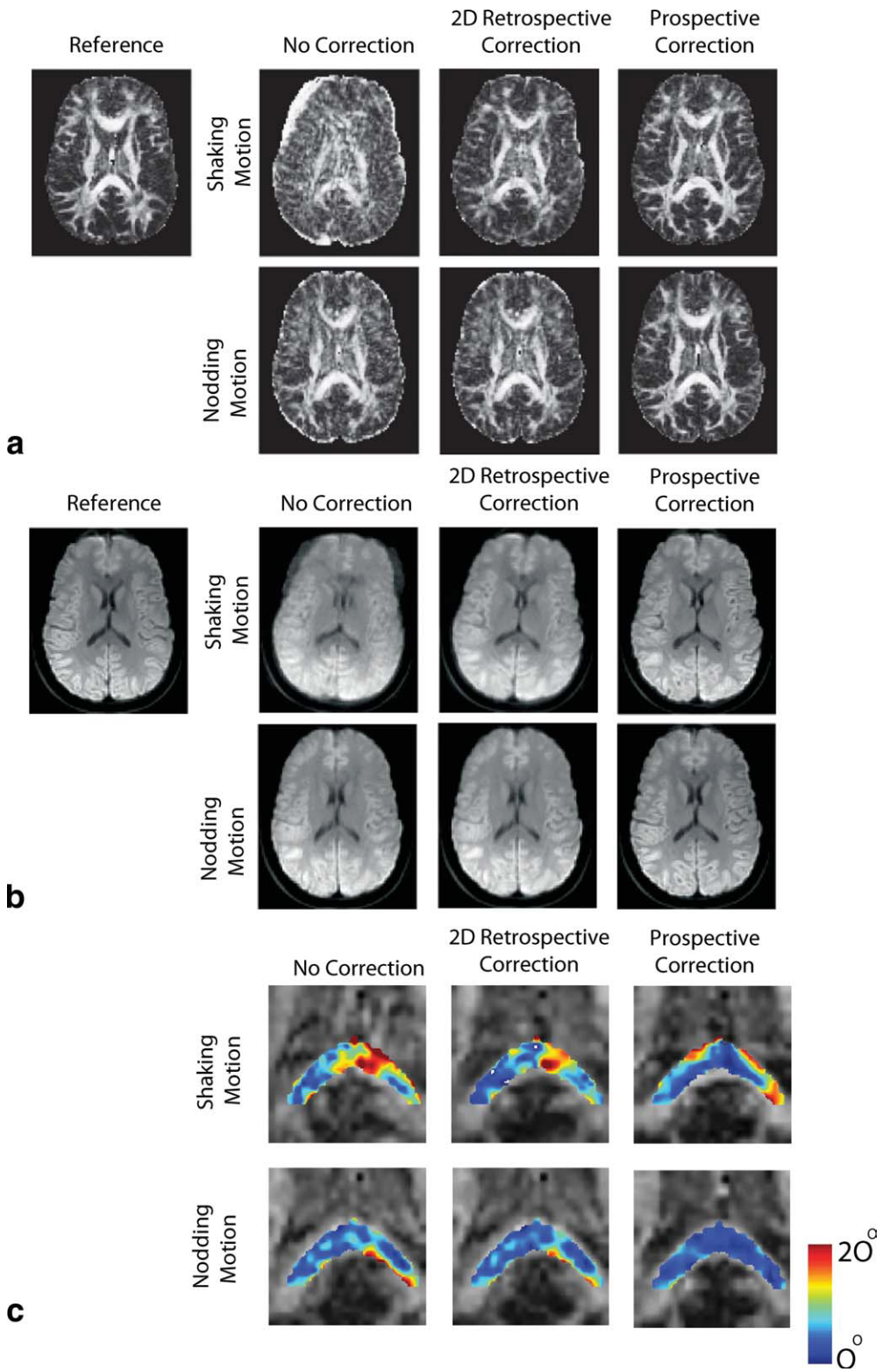

FIG. 4. Results of in vivo DTI experiments with 128 × 128 resolution. Reconstructed FA maps (**a**) and isotropic DWI images (**b**) with and without 2D retrospective and prospective correction in the presence of shaking and nodding motion are shown. It can be seen that in the presence of random head motion the resulting images show significant motion-related artifacts if optical motion tracking was turned off. These artifacts were largely removed after motion tracking was turned on. Superiority of prospective correction over retrospective method is better demonstrated in the presence of nodding motion. In this case, retrospective correction did not improve image quality because of the inability of this method to correct for through-plane motion, whereas prospectively corrected image looks very similar to the reference. The differences in structure between the reference FA map and the motion-corrected maps are due to the fact that the subject did not return to the original position between "no motion" and "motion" scans. The angular deviation maps of the major eigenvectors from true orientations are shown in (**c**). True orientations are given by the data set with no motion. Prospective correction provided eigenvectors with lower deviation compared to retrospective correction for both cases. [Color figure can be viewed in the online issue, which is available at wileyonlinelibrary.com.]

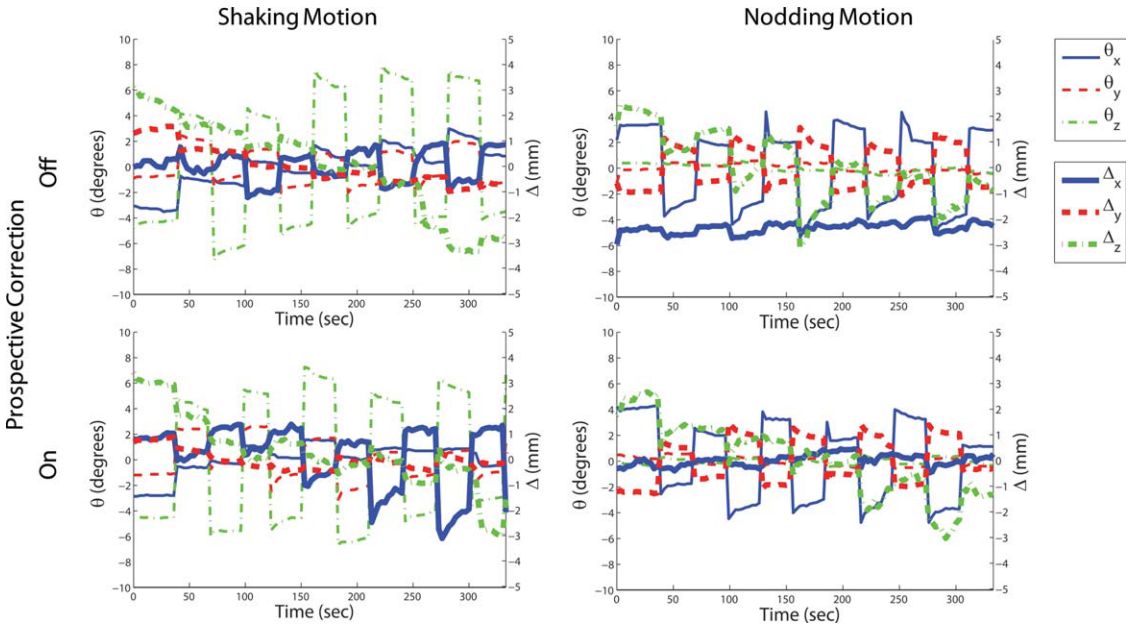

FIG. 5. Motion plots corresponding to the shaking and nodding motion experiments in Fig. 4. The motion performed by the patient was similar for both scans when the motion tracking was turned off and on. [Color figure can be viewed in the online issue, which is available at wileyonlinelibrary.com.]

box and whisker plots of the correlation coefficients for navigator images that were obtained with each interleave. For both in-plane and nodding motion, the performance of prospective correction was better than retrospective correction, as given by the higher correlation coefficient between the navigators.

Variance Maps

Figure 6b shows the pixel-by-pixel variance of signal intensity throughout the 16 $b = 0$ images. Without motion correction a large pixel variance was seen, especially at the edges of the brain. Pixel variance was lowest when prospective motion correction was applied.

Due to the high sensitivity of the diffusion weighting to motion, any motion during the diffusion-weighting period results in irrecoverable signal loss and presents a limitation for any motion correction technique. This is shown in Fig. 7. The presence of patient motion (Fig. 7a) results in a decrease in average signal intensity in the corresponding navigator data (Fig. 7b). This motion-related signal loss can be attributed to signal dephasing (Fig. 7b) and is also evident when looking at the corresponding navigator images (Fig. 7c). To account for data corruption caused by motion during the diffusion preparation period, a rescanning strategy was employed wherein, if motion detected by the optical system was larger than a set threshold (1 mm and 1° for this study), a number of recently acquired *k*-space segments were reacquired. To reflect the true scenario for retrospective motion correction, no rescanning data were used for the tensor reconstruction from measurements performed with either no motion correction or retrospective correction.

In Vivo DWI Experiments, 256 × 256 Resolution, Multishot

Figure 8a shows high-resolution isotropic diffusion-weighted images acquired without and with subject motion. Figure 8b shows the motion plots detected by the optical system. The image quality metric based on high frequency spectrum energy is shown in Fig. 8c, where greater high frequency power implies less motion artifacts (8). Similar to the previous in vivo experiment, the data set with motion and without motion correction showed detrimental motion artifacts. Two-dimensional retrospective correction was successful in removing some of the artifacts; however, some artifacts remained due to the existence of through-plane motion. The best image quality in the presence of motion was obtained with prospective correction. Also, the total high frequency power for no motion and prospective correction was close to one for all slices (Fig. 8c), which demonstrates that the image quality of the resting scan was not degraded by prospective motion correction.

DISCUSSION

The ever-increasing complexity of DTI studies leads to very long scan times and an increased chance of patient

Table 1
Mean Angular Deviation of Major Eigenvectors from True Orientations Inside an ROI Enclosing the Splenium of the Corpus Callosum Containing 89 pixels (shown in Fig. 4c)

	No correction	Retrospective	Prospective
Shaking motion	10.14 ± 6.32	7.38 ± 4.99	7.02 ± 4.81
Nodding motion	6.02 ± 3.83	5.30 ± 2.99	3.29 ± 1.63

The true orientations were defined by the no motion and no correction scan.

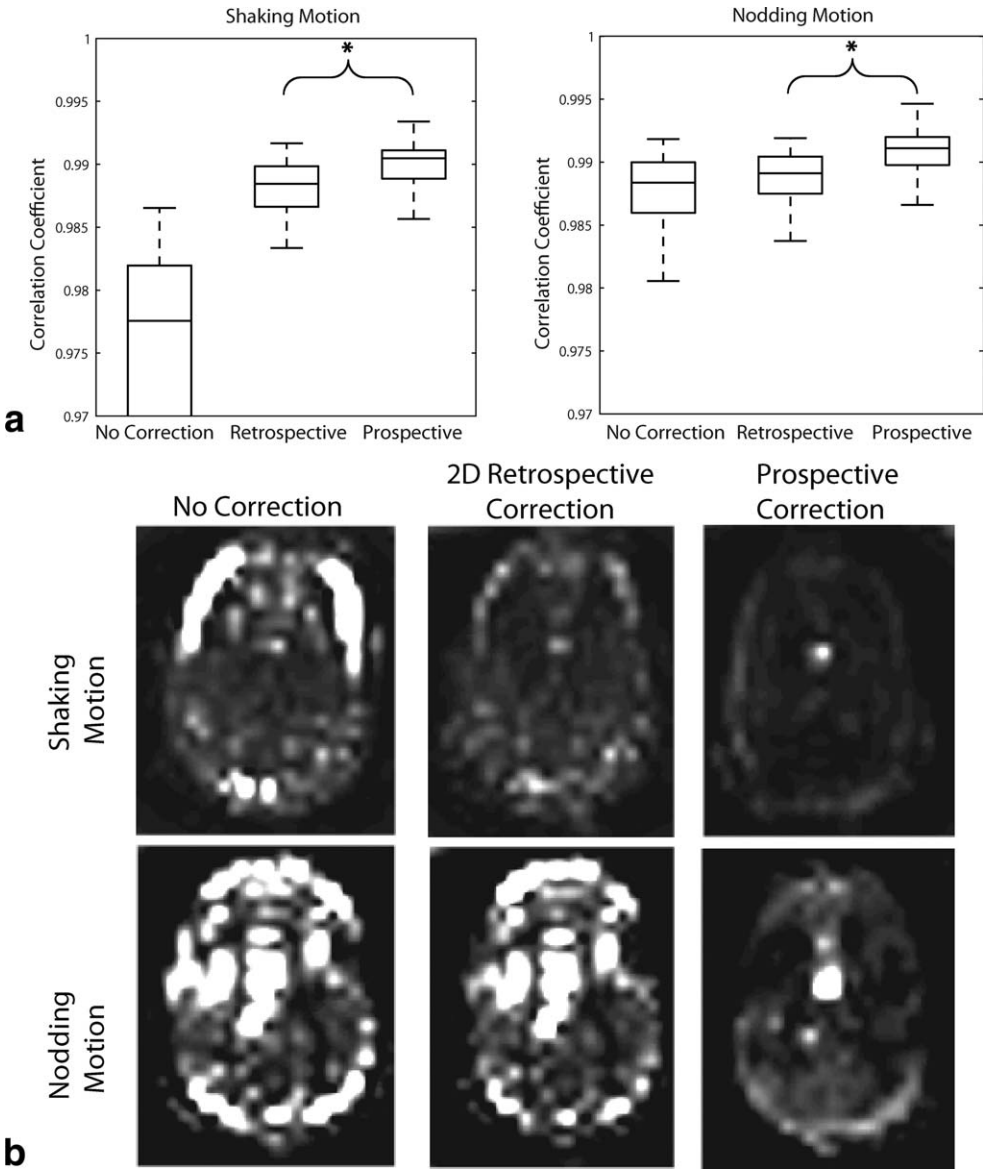

FIG. 6. **a**: Correlation coefficients of each navigator with the template for the three different methods. The higher correlation coefficient obtained while using prospective motion correction compared to retrospective correction implies that the navigator images are more "similar" to each other when prospective correction was used. **b**: Pixel-by-pixel variance maps throughout the $b = 0$ images (16 images). In the nodding motion case, prospective correction was much successful in reducing the variation between navigators. The bright spot visible in the lower three images is due to pulsation of the lateral ventricle. [Color figure can be viewed in the online issue, which is available at wileyonlinelibrary.com.]

motion. Head motion correction is therefore very important for DTI. Although the chances of head motion is higher for certain patient populations (e.g., stroke or Parkinson's disease patients), head motion can be observed even for highly cooperative subjects (3) due to the excessively long acquisition times seen with DTI.

The vast majority of motion correction methods used for single and multishot DTI apply retrospective processing techniques (1,2,5,6,24–27). There are considerable shortcomings associated with retrospective approaches, which were addressed in this work by a monovision-based optical tracking system and an adaptive prospective motion correction approach. Unlike other in-bore optical tracking systems that have been introduced previously (12), the system presented here uses a single camera, which eliminates the necessity to perform extrinsic stereo calibration. The novel marker design used in this study allowed for accurate tracking of large head motions, with minimum latency between the instance of motion in the camera and the scan plane update in response to the pose changes.

In general, prospective methods that use external tracking devices have been proposed to perform six degree-of-freedom head motion correction with little or no change in the pulse sequence. Zaitsev et al. (10) used a stereovision system that had been placed outside the scanner bore to track and correct for rigid head motion. Despite compelling results, the aforementioned method also faced some challenges: (1) due to the distance between the cameras and the marker, the system required very high accuracy, which in turn required careful and tedious scanner–camera cross-calibration; (2) the line-of-sight between the cameras and the self-reflecting marker can be obstructed due to longer bore size (e.g., 7 T) or a patient's larger girth. To alleviate these difficulties, stereovision systems were placed inside the scanner bore (11,12,15). The advantage of an in-bore system compared to an out-of-bore set-up is that there are no obstructions between the camera and the

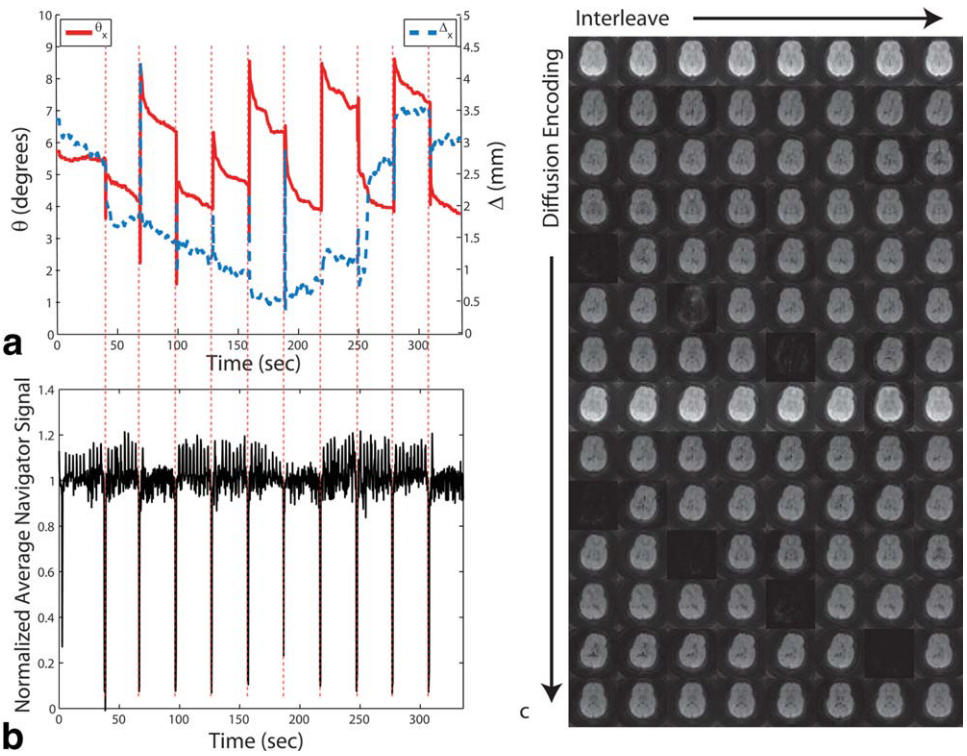

FIG. 7. Navigator signal loss due to motion. Due to the motion sensitivity of the diffusion-weighting gradients, patient motion during the diffusion-preparation period causes irrecoverable signal dropouts. This is clearly visible from the navigator signal that was obtained from the spiral-in readout. It can be seen that whenever there is patient motion (**a**), the navigator signal was significantly reduced. Only the dominant motion axes (i.e., θ_x and Δx) are shown to simplify the graph. Example navigator images from one slice are shown at the right (**c**). [Color figure can be viewed in the online issue, which is available at wileyonlinelibrary.com.]

object being tracked. Due to the proximity of the camera, several aspects still need to be considered: (1) replacing magnetic parts of the video imager with nonmagnetic components; (2) preventing RF noise of the video imager from leaking into the RF chain; (3) preventing the imager itself from perturbing the amplitude of (excitation) radiofrequency field; and (4) preventing the RF transmit from affecting the video signal. A major benefit of the approach used in this study was that no extrinsic stereocalibration was needed as there was a single camera, and the cross-calibration between MR scanner and the camera coordinate system was fast (~ 60 sec) and could be carried out with the patient inside the scanner. A potential challenge could be the accuracy of position detection of agar droplets (used for cross-calibration) due to off-resonance. One of the strengths of the calibration approach used for this study is the fitting of a spatial grid pattern to the measured MR-visible droplet tessellation. Similar to registration, accuracy and precision can be improved by using a large number of pixels and droplets and, thus, cross-calibration errors due to local field inhomogeneities can be reduced to an insignificant level (Fig. 2).

It has been shown that depending on the desired image resolution and signal-to-noise ratio (SNR), tracking precision must be better than a voxel size (28). High precision is important to guarantee that the image quality is not degraded when the subject is staying still. In our experiments, we observed that prospective motion correction of "nonmotion" data did not degrade the image quality of single-shot DTI (Fig. 3) and high-resolution in vivo DWI scans (Fig. 8a,c). In terms of accuracy and precision requirements, an advantage of using external tracking systems is that the performance can be improved independent of the MR scanning process by choosing better hardware (e.g., better optics to give sharper images). Alternatively, it is possible to improve precision by averaging the motion signal or using Kalman filtering (29).

The mounting of the marker on the patient is also an important consideration to guarantee both patient comfort and adequate tracking accuracy. In this study, the marker was mounted on the forehead using Velcro straps. The forehead is a good location to place the marker as the rigidity assumption between the marker and the brain becomes invalid only for frowning motions. Even in the presence of frowning motion, the marker will go back to its original position after the frowning motion is complete and is usually not a persistent state. Thus, we do not expect the rigidity between the marker and the head to become invalid except for rare cases.

In this study, it has been shown that the performance of prospective optical motion correction was better compared to retrospective 3D volume-to-volume realignment or retrospective navigator-based 2D correction. Advantages of using prospective optical motion correction can be summarized as follows:

Through-Plane Motion

A profound shortcoming of retrospective motion correction methods is its inability to correct for through-plane motion. The prospective approach maintained slice position with respect to the patient frame-of-reference and assured data consistency. This approach eliminated issues resulting from through-plane motion. The benefits of prospective motion correction over retrospective methods have been shown in in vivo experiments of this study. Specifically, it was observed that in the presence

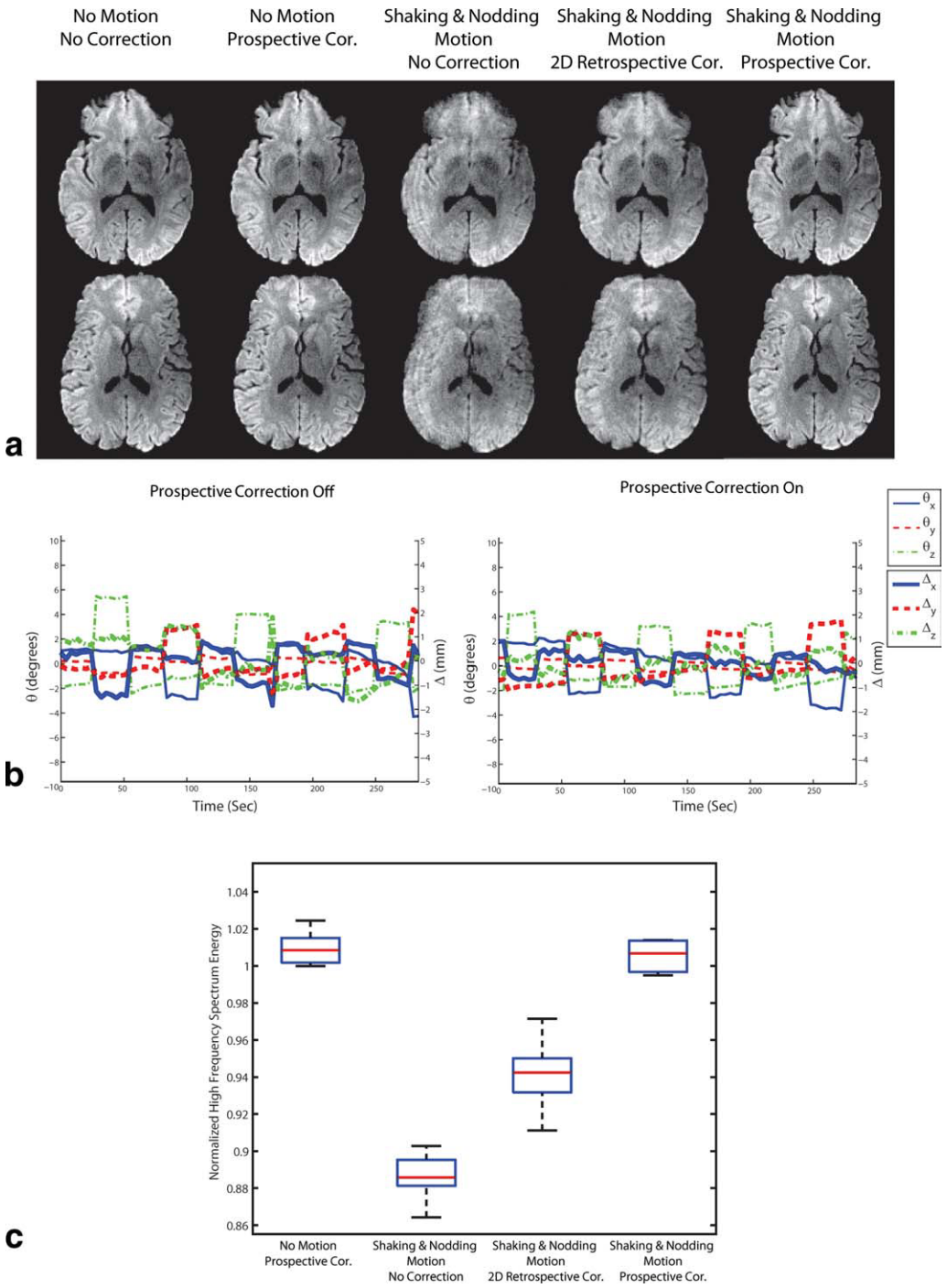

FIG. 8. Results of high resolution DWI experiments with resolution 256 × 256. Similar to the in vivo experiments with 128 × 128 resolution, prospective motion correction performed better compared to retrospective correction due to the existence of through-plane motion. The motion plots are shown in (**b**). The distribution of high frequency spectrum energy for seven slices in the acquisition is shown in (**c**). For all slices shown, the images with prospective correction had higher energy at high frequencies compared to uncorrected or retrospectively corrected images, implying less motion artifacts. [Color figure can be viewed in the online issue, which is available at wileyonlinelibrary.com.]

of through-plane motion (e.g., predominantly nodding motion), retrospective motion correction was ineffective at removing motion artifacts, whereas most of the artifacts were removed with prospective correction (Figs. 3, 4, 6, and 8).

k-space Undersampling due to Rotational Motion

Retrospective correction of rotational motion can also leave gaps in *k*-space, which causes undersampling artifacts (21). If prospective methods are used, the scanner geometry is updated before data readout takes place.

Thus, aliasing artifacts from local *k*-space undersampling are not an issue.

Signal Loss due to Motion during Diffusion-Preparation Period

Due to the sensitivity of diffusion-weighting gradients to small motion, gross head motion during the diffusion-preparation period results in irrecoverable signal loss (Fig. 7; Ref. 14). Retrospective compensation methods are limited to identifying and discarding this potentially corrupted data. However, data elimination may result in undersampling of *k*-space, which, in turn, may impair the quality of the diffusion-weighted images. Eliminating corrupted data is also a common policy for single-shot scans, which can go unnoticed if there are an excessive number of diffusion directions or signal averages. However, for a borderline number of directions, such as for higher resolution scans, data elimination might severely impair the estimation of the tensor. Another possible challenge with retrospectively discarding data is that the detection of corrupted slices using image-based metrics (mean signal intensity or entropy) becomes unreliable if the image SNR is low. This was the case for inferior slices in the single-shot EPI DTI scan; due to their low SNR, some of these corrupted slices were mistakenly included in the DTI analysis. This caused significant artifacts in FA maps, and missing visualization of the cortico-spinal tracts (Fig. 3a,b). With our prospective approach, a rescanning strategy was implemented whereby data was reacquired if the detected motion exceeded a certain threshold, which eliminated the problems with retrospectively discarding data. However, for the high resolution scans, subject movement was not frequent enough to cause significant undersampling in *k*-space (Figs. 5 and 8b). Thus, the artifacts seen in the retrospectively corrected images of Figs. 4a,b and 8a were mainly due to misregistration.

Change in Effective Diffusion-Encoding Direction

As described in the Introduction section, rotational head motion causes the effective diffusion-encoding direction to change (1). Correcting the **b** matrix is therefore necessary to get accurate fiber tracts (3). In the current system, the scanner geometry was updated in real-time before the diffusion-preparation period. Thus, the diffusion-encoding directions played out were always the same with respect to the patient frame of reference. This eliminated entirely the aforementioned difficulties that might result from **b** matrix alterations and varying diffusion-encoding directions throughout successive interleaves.

Partial Volume Artifacts

For the high-resolution scans used in this study, the slice thickness was rather large (5 mm) to obtain adequate SNR. With thicker slices, the ability of retrospective image-based methods to resolve partial volume artifacts decreases. This can impact the performance of slice-to-volume registration methods where the slice thickness must be lower than a certain threshold to provide sufficient sampling coverage in 3D space (2). Image-based methods are expected to work better with thinner slices, but the low SNR due to decreased slice thickness can be a challenge. The performance of optical prospective motion correction to resolve partial volume artifacts is independent of the slice thickness.

In general, another advantage of using an external optical tracking system is that it eliminates the necessity to obtain MR navigator data for motion correction, thus providing more sequence design flexibility. However, for the high-resolution scans performed in this study, 2D spiral-in navigators were used for both phase and motion correction. In this context, it must be noted that, for high-resolution DWI and DTI, the primary purpose of optical tracking is not eliminating the need to use navigator data. Even if 2D navigator data is available, it is better to use the optical tracking system due to the reasons described above; the most important of which is through-plane motion. Nonlinear phase correction could have been done also by using the central part of a variable density spiral (5), but would not have provided the navigator data for our study to simultaneously compare the optical approach against retrospective/navigator-based methods.

Despite prospective motion correction, a challenge that remains is the variation of receiver coil sensitivity relative to the patient frame of reference. This becomes increasingly important for larger motion or smaller coil elements (30,31) and needs to be considered for parallel imaging. A remedy has been described in Ref. 21 and may be incorporated into a nonlinear phase correction parallel imaging algorithm (20), but its validation together with prospective motion correction was beyond the scope of this study.

CONCLUSIONS

An optical tracking system was presented to correct for rigid head motion for DTI. The system uses a single camera mounted on the head coil and a self-encoded marker. The setup and cross-calibration of the system was fast (<1 min), which is important for clinical applicability of such systems. Initial in vivo results showed that the proposed system performed superior to retrospective motion correction, especially when through-plane motion was present.

ACKNOWLEDGMENTS

We would like to thank Melvyn Ooi for helping with data analysis and Rafael O'Halloran and Daniel Kopeinigg for helping with the data acquisition.

REFERENCES

1. Rohde GK, Barnett AS, Basser PJ, Marenco S, Pierpaoli C. Comprehensive approach for correction of motion and distortion in diffusion-weighted MRI. Magn Reson Med 2004;51:103–114.
2. Jiang S, Xue H, Counsell S, Anjari M, Allsop J, Rutherford M, Rueckert D, Hajnal JV. Diffusion tensor imaging (DTI) of the brain in moving subjects: application to in-utero fetal and ex-utero studies. Magn Reson Med 2009;62:645–655.
3. Leemans A, Jones DK. The B-matrix must be rotated when correcting for subject motion in DTI data. Magn Reson Med 2009;61:1336–1349.

4. Pipe JG. Motion correction with PROPELLER MRI: application to head motion and free-breathing cardiac imaging. Magn Reson Med 1999;42:963–969.
5. Liu C, Bammer R, Kim DH, Moseley ME. Self-navigated interleaved spiral (SNAILS): application to high-resolution diffusion tensor imaging. Magn Reson Med 2004;52:1388–1396.
6. Aksoy M, Liu C, Moseley ME, Bammer R. Single-step nonlinear diffusion tensor estimation in the presence of microscopic and macroscopic motion. Magn Reson Med 2008;59:1138–1150.
7. Speck O, Hennig J, Zaitsev M. Prospective real-time slice-by-slice motion correction for fMRI in freely moving subjects. MAGMA 2006;19:55–61.
8. Ooi MB, Krueger S, Thomas WJ, Swaminathan SV, Brown TR. Prospective real-time correction for arbitrary head motion using active markers. Magn Reson Med 2009;62:943–954.
9. Thesen S, Heid O, Mueller E, Schad LR. Prospective acquisition correction for head motion with image-based tracking for real-time fMRI. Magn Reson Med 2000;44:457–465.
10. Zaitsev M, Dold C, Sakas G, Hennig J, Speck O. Magnetic resonance imaging of freely moving objects: prospective real-time motion correction using an external optical motion tracking system. Neuroimage 2006;31:1038–1050.
11. Bammer R. Apparatus and method for real-time motion-compensated magnetic resonance imaging. US Patent Application No.11/823469, Publication No. 20090209846, Published August 20, 2009.
12. Qin L, van Gelderen P, Derbyshire JA, Jin F, Lee J, de Zwart JA, Tao Y, Duyn JH. Prospective head-movement correction for high-resolution MRI using an in-bore optical tracking system. Magn Reson Med 2009;62:924–934.
13. Ooi MB, Krueger S, Thomas WJ, Brown TR. Real-time intra-volume motion correction in EPI using active markers. Proceedings of the Joint Annual Meeting of ISMRM & ESMRMB, Stockholm, Sweden; 2010. p 5038.
14. Anderson AW, Gore JC. Analysis and correction of motion artifacts in diffusion weighted imaging. Magn Reson Med 1994;32:379–387.
15. Aksoy M, Newbould R, Straka M, Holdsworth S, Skare S, Santos J, Bammer R. A real time optical motion correction system using a single camera and 2D marker. Proceedings of the 16th Scientific Meeting of ISMRM; Toronto, Canada; 2008. p 3120.
16. Forman C, Aksoy M, Hornegger J, Bammer R. Self-encoded marker for optical prospective head motion correction in MRI. Med Image Comput Comput Assist Interven 2010;13:259–266.
17. Hartley R, Zisserman A. Multiple view geometry in computer vision. Cambridge: Cambridge University Press; 2003.
18. Uematsu Y, Saito H. Improvement of accuracy for 2D marker-based tracking using particle filter. Proceedings of the 17th International Conference on Artificial Reality and Telexistence; 2007; Esbjerg, Denmark. pp 183–189.
19. Aksoy M, Acar B, Bammer R. SNR Dependence of DTI fiber tracking protocols. ISMRM Workshop on Diffusion MRI, Lake Louise, Canada; 2005.
20. Liu C, Moseley ME, Bammer R. Simultaneous phase correction and SENSE reconstruction for navigated multi-shot DWI with non-cartesian k-space sampling. Magn Reson Med 2005;54:1412–1422.
21. Bammer R, Aksoy M, Liu C. Augmented generalized SENSE reconstruction to correct for rigid body motion. Magn Reson Med 2007;57:90–102.
22. Kim DH, Adalsteinsson E, Spielman DM. Simple analytic variable density spiral design. Magn Reson Med 2003;50:214–219.
23. Skare S, Newbould RD, Clayton DB, Bammer R. Propeller EPI in the other direction. Magn Reson Med 2006;55:1298–1307.
24. Atkinson D, Porter DA, Hill DL, Calamante F, Connelly A. Sampling and reconstruction effects due to motion in diffusion-weighted interleaved echo planar imaging. Magn Reson Med 2000;44:101–109.
25. Butts K, de Crespigny A, Pauly JM, Moseley M. Diffusion-weighted interleaved echo-planar imaging with a pair of orthogonal navigator echoes. Magn Reson Med 1996;35:763–770.
26. Miller KL, Pauly JM. Nonlinear phase correction for navigated diffusion imaging. Magn Reson Med 2003;50:343–353.
27. Pipe JG, Farthing VG, Forbes KP. Multishot diffusion-weighted FSE using PROPELLER MRI. Magn Reson Med 2002;47:42–52.
28. Maclaren J, Speck O, Stucht D, Schulze P, Hennig J, Zaitsev M. Navigator accuracy requirements for prospective motion correction. Magn Reson Med 2009;63:162–170.
29. Maclaren J, Speck O, Hennig J, Zaitsev M. A Kalman filtering framework for prospective motion correction. Proceedings of the 17th Scientific Meeting of ISMRM, Honolulu, HI; 2009. p 4602.
30. Aksoy M, Bammer R. Effect of motion-induced altered coil sensitivity on parallel imaging performance. Proceedings of the 16th Annual Meeting of ISMRM, Toronto, Canada; 2008. p 3111.
31. Luengviriya C, Stucht D, Schulze P, Yun J, Danishad K, Kadashevich I, Speck O. Necessity of sensitivity map correction in motion correction at 7T MRI. ISMRM Workshop on Current Concepts of Motion Correction for MRI & MRS, Kitzbühel, Tyrol, Austria; 2010.